Article

Zeylleucapenoids A−D, Highly Oxygenated Diterpenoids with Anti-inflammatory Activity from *Leucas zeylanica*

Ting Zhao[†,a,b], Xuan Zhang[†,a,b], Xu-Hua Nong[a,b], Xue-Ming Zhou[a,b], Ru-Ru Chai[a,b], Xiao-Bao Li[a,b*] and Guang-Ying Chen[a,b*]

[1] Key Laboratory of Tropical Medicinal Resource Chemistry of Ministry of Education Hainan Normal University, Haikou, Hainan 571158, China
[2] Key Laboratory of Tropical Medicinal Plant Chemistry of Hainan Province, College of Chemistry and Chemical Engineering, Hainan Normal University, Haikou, Hainan 571158, China
* Correspondence: chgying123@163.com (G.-Y. Chen), lixiaobao0797@163.com (X.-B. Li)
† These authors contributed equally to this work.

Abstract: Four previously undescribed highly oxygenated diterpenoids (**1–4**), zeylleucapenoids A–D, characterized by halimane and labdane skeletons, were isolated from the aerial parts of *Leucas zeylanica*. Their structures were elucidated primarily by NMR experiments. The absolute configuration of **1** was established by theoretical ECD calculations and X-ray crystallographic analysis, whereas those for **2**−**4** were assigned by theoretical ORD calculations. Zeylleucapenoid D (**4**), with an IC_{50} value of 38.45 μM in RAW264.7 macrophages and nontoxic activity for zebrafish embryo, and obviously inhibited pro-inflammatory cytokines TNF-α and IL-6 in a dose-dependent manner. Compound **4** inhibited of the expression of inducible nitric oxide synthase (iNOS) and cyclooxygenase-2 (COX-2). Furthermore, molecular docking analysis indicated the possible mechanism of action for **4** may be bind to targets by hydrogen- and hydrophobic- bond interactions.

Keywords: *Leucas zeylanica*; Highly oxygenated; Diterpenoids; Anti-inflammatory activity; Molecular docking; Zebrafish model

1. Introduction

Inflammation has been closely related to the immune defense response of the patients with chronic diseases[1-2]. Discovery of new anti-inflammatory agents was hopeful to treatment of inflammation-linked diseases, such as metabolic syndromes, autoimmune, and so on. Medicinal plants were an important source for development of lead drugs. Hitherto, investigation of the chemical constituents of medicinal plants have attracted much attentions from chemists. Diterpenoids are a large group of naturally occurring chemical constituents found in terrestrial plants, microbes, insects, and marine organisms[3-4], which exhibited a wide variety of bioactivities, such as anti-inflammatory, antimicrobial, antitumor, and analgesic activities[5-6].

Leucas species are perennial herbs and distributed mainly in East Africa and subtropical area of Asia[7]. There are about 125 *Leucas* species globally, of which seven species grow in the southern China. The studies for a few species led to the isolation of diterpenoids as active constituents, which exhibited anti-inflammatory and anti-mycobacterial activities[8-9]. The aerial parts of *L. zeylanica* have been used as a folk medicine in treating inflammatory diseases, e.g., pertussis, asthma, headache and indigestion[10].

Preprints (www.preprints.org) | NOT PEER-REVIEWED | Posted: 9 May 2023 doi:10.20944/preprints202305.0651.v1

Our previous chemical investigations on *L. zeylanica* led to the identification of labdane diterpenoids and flavonoids[11]. In search for novel, bioactive, and structurally diverse natural products from the traditional Chinese folk medicine, four undescribed highly oxygenated diterpenoids **1-4**, were isolated from the aerial parts of *L. zeylanica*. Among them, compound **1** was elucidated to be a halimane-type diterpenoid, while **2-4** were labdane-type diterpenoids **(Figure 1).** Here, we report the structures, anti-inflammatory effects and the potential mechanisms of the isolated diterpenoids.

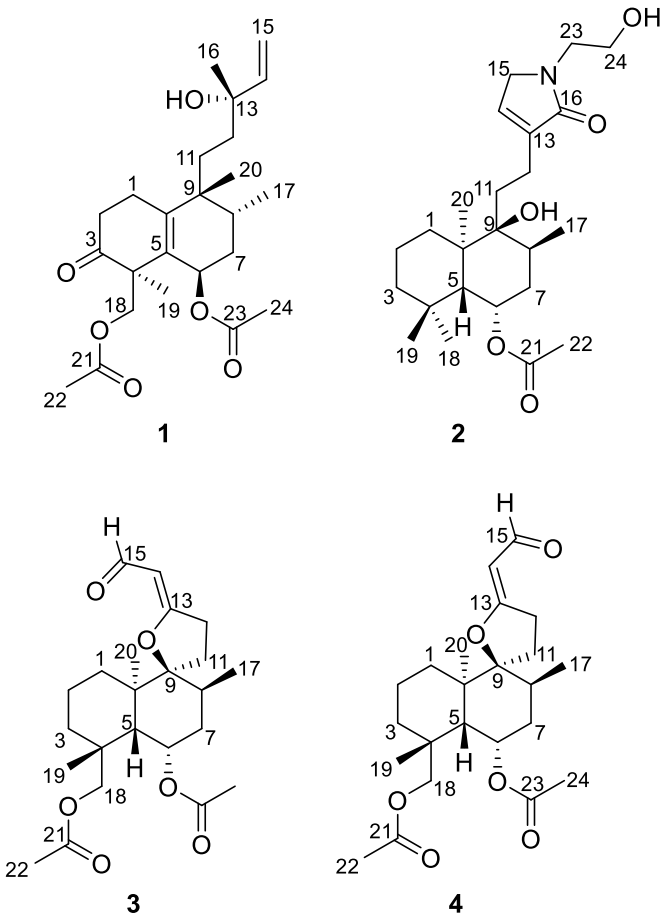

Figure 1 Structures of compounds **1-4** from *L. zeylanica*.

2. Results and Discussion

*2.1. Elucidation of the Chemical Structures of zeylleucapenoids A-D (**1-4**).*

Zeylleucapenoids A (**1**) was obtained as colorless crystals. Analysis of the HR-ESI-MS spectrum showed it had a molecular formula of $C_{24}H_{36}O_6$, indicating seven degrees of unsaturation. The ^{1}H and ^{13}C-NMR spectral data of **1** (**Table 1**) suggested that they were very similar to those of Leucasperone B[12], except that the absence of an oxygenated methine at (δ_H 4.15/δ_C 71.3, CH) in Leucasperone B, and the additional presence of a methylene at (δ_H 1.56/δ_C 30.0, CH_2) in **1**. Based on this, compound **1** was considered as an analogue of Leucasperone B. Further the COSY cross-peak between H_2-11/H_2-12 confirmed that the methine of C-11 in Leucasperone B was replaced by a methylene in **1**, which was supported by the key HMBC correlations from H_2-11 to C-8/C-10/C-13, and from both H-8 and H_3-20 to C-10/C-11 (**Figure 2**). The partial relative configuration of **1** was determined by NOESY correlations showing cross-peaks between both H-6 and Me-17 with Me-19, H-8 with Me-20, which indicated H-6 and Me-19 were on the same orientation, while H-8 and Me-20 were on another orientation. Finally, a comparison of the experimental and

Preprints (www.preprints.org) | NOT PEER-REVIEWED | Posted: 9 May 2023 doi:10.20944/preprints202305.0651.v1

calculated ECD spectra of **1** suggested that the absolute configuration of C-4/C-6/-C-8/C-9 in **1** was as 4*S*,6*R*,8*R*,9*R*, attributing to the spectrum of isomer (4*S*,6*R*,8*R*,9*R*)-**1** showed a similar trend with the experimental curve (**Figure 4**). However, the absolute configuration of C-13 in **1** was still not assigned. Fortunately, the single crystal of **1** was attained and the absolute configuration of **1** (**Figure 5**) was clearly defined to be (4*S*,6*R*,8*R*,9*R*,13*S*) by X-ray diffraction analysis (CCDC No. 2225700), and named as zeylleucapenoid A.

Compound **2** was purified as white powder. Its molecular formula $C_{24}H_{39}NO_5$ was defined by HR-ESI-MS spectrum with an ion peak at *m*/*z* 444.2725 $[M+Na]^+$ (calcd for $C_{24}H_{39}NO_5Na$, 444.2726), corresponding to six degrees of unsaturation. The ^1H NMR data of **2** (**Table 1**) showed characteristic resonances for an olefinic proton at δ_H 6.79 (H-14), three methines including an oxygenated proton at δ_H 5.23 (H-6), and five methyls at δ_H 0.85 (H-17), 0.88 (H-19), 0.94 (H-18), 1.19 (H-20) and 1.98 (H-22). The ^{13}C NMR spectrum (**Table 1**) exhibited totally 24 carbon signals, including two amide/ester carbonyls at δ_C 170.8 (C-16)/169.9 (C-21), two sp^2 carbons at δ_C 139.5 (C-13)/135.3 (C-14), four methyls at δ_C 33.4 (C-19)/23.5 (C-18)/21.6 (C-22)/16.0 (C-17), three sp^3 methines at δ_C 69.5 (C-6)/46.7 (C-5)/31.1 (C-8), three sp^3 quaternary carbons at δ_C 75.6 (C-9)/43.4 (C-10)/33.5 (C-4), and nine methylenes. These spectral data indicated that **2** was an analogue of vitexlactam A[13], except for the additional existence of an ethoxy moiety in **2**. Further analysis of 2D-NMR spectra of **2** confirmed the assignment above. In the COSY spectrum, the correlation between H_2-23 and H_2-24 was observable. In the HMBC spectrum, there were long-range correlations from H_2-15 to C-23, and from H_2-23 to C-15/C-16 (**Figure 2**), which suggested that the ethoxy moiety was connected to the nitrogen-atom. The relative configuration of **2** was determined the same as vitexlactam A by observation of NOESY correlations (**Figure 3**). In the NOESY spectrum, there were cross-peaks between Me-20 with H-8/H_2-11/Me-18, indicating they were on α-cofacial, while H-5/H-6/Me-19/9-OH were on β-cofacial. The absolute configuration of **2** was determined to be 5*R*/6*S*/8*S*/9*S*/10*R* by comparison of its specific rotation $[\alpha]^{25}_D$ +51.7 (*c* 2.1, MeOH) with that of vitexlactam A $[\alpha]^{25}_D$ –10.7 (*c* 0.42, $CHCl_3$)[13], showing an opposite sign. Furthermore, comparison of the calculated optical rotatory dispersion (ORD) spectrum of **2** with the experimental one also supported that assignment, in which the calculated ORD spectrum of 5*R*,6*S*,8*S*,9*S*,10*R*-**2** agreed well with the experimental curve for **2** (**Figure 6**). Thus, **2** was elucidated as shown in **Figure 1**, and named as zeylleucapenoid B.

Table 1. ^1H and ^{13}C NMR spectral data of compounds **1**–**2**

Position	**1**[a]		**2**[b]	
	δ_H, Mult, (*J* in Hz)	δ_C	δ_H, Mult, (*J* in Hz)	δ_C
1	2.47, m; 2.59, m	24.2	1.34, m; 1.59, m	35.9
2	2.51, m	38.4	1.41, m	18.4
			1.55, m	
3	-	214.7	1.10, m; 1.24, m	44.5
4	-	52.1	-	33.5
5	-	130.3	1.68, d, (2.4)	46.7
6	5.43, t, (2.8)	68.5	5.23, dd, (5.6, 2.8)	69.5
7	1.71, m	36.0	1.35, m	32.2
			1.62, m	
8	1.85, m	34.5	2.02, m	31.1
9	-	42.6	-	75.6
10	-	149.8	-	43.4
11	1.56, m	30.0	1.37, m	33.0

Preprints (www.preprints.org) | NOT PEER-REVIEWED | Posted: 9 May 2023 doi:10.20944/preprints202305.0651.v1

			1.57, m	
12	1.21, m	40.4	2.23, t, (7.2)	22.5
	1.63, m			
13	-	73.9	-	139.5
14	5.87, dd, (17.6, 10.8)	146.2	6.79, s	135.3
15	5.05, dd, (10.8, 2.0)	112.4	3.96, s	51.5
	5.20, dd, (17.6, 2.0)			
16	1.15, s	27.7	-	170.8
17	1.04, d, (7.2)	16.6	0.85, d, (6.8)	16.0
18	4.05, d, (10.8)	69.5	0.94, s	23.5
	4.20, d, (10.8)			
19	1.18, s	20.1	0.88, s	33.4
20	1.24, s	27.5	1.19, s	19.0
21	-	172.2	-	169.9
22	1.98, s	20.7	1.98, s	21.6
23	-	172.4	3.38, t, (5.8)	43.5
24	2.00, s	21.5	3.50, t, (5.8)	59.5

[a] measured in CD_3OD at 400 MHz, [b] measured in DMSO-d_6 at 400MHz.

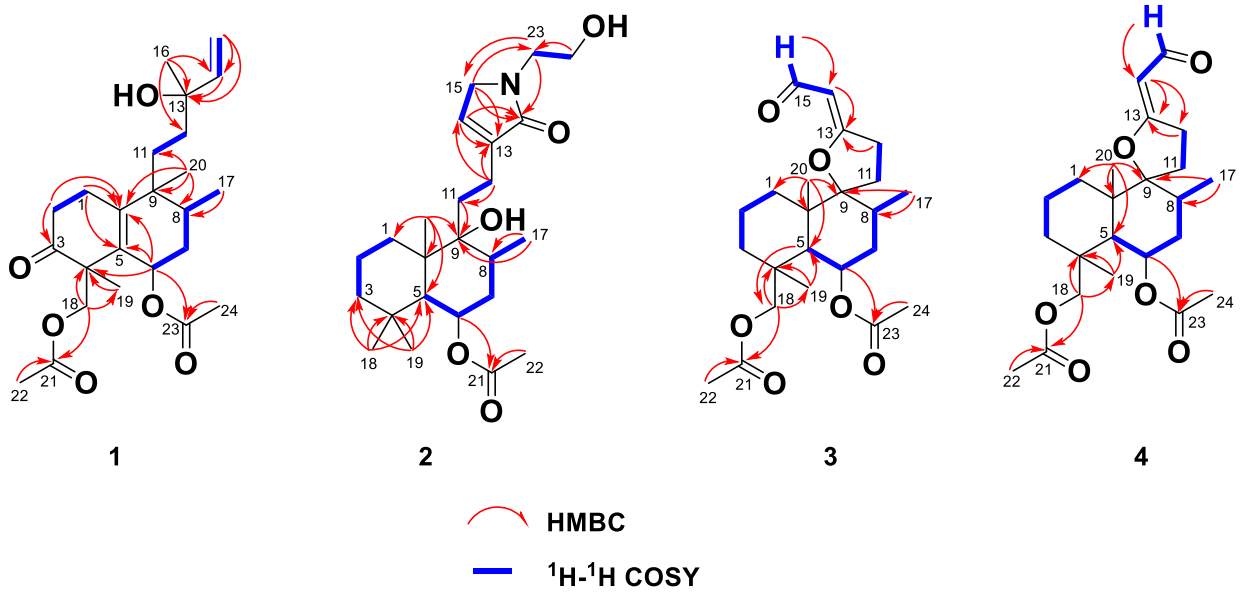

Figure 2 Key HMBC and ^1H-^1H COSY correlations of **1-4**.

Preprints (www.preprints.org) | NOT PEER-REVIEWED | Posted: 9 May 2023 doi:10.20944/preprints202305.0651.v1

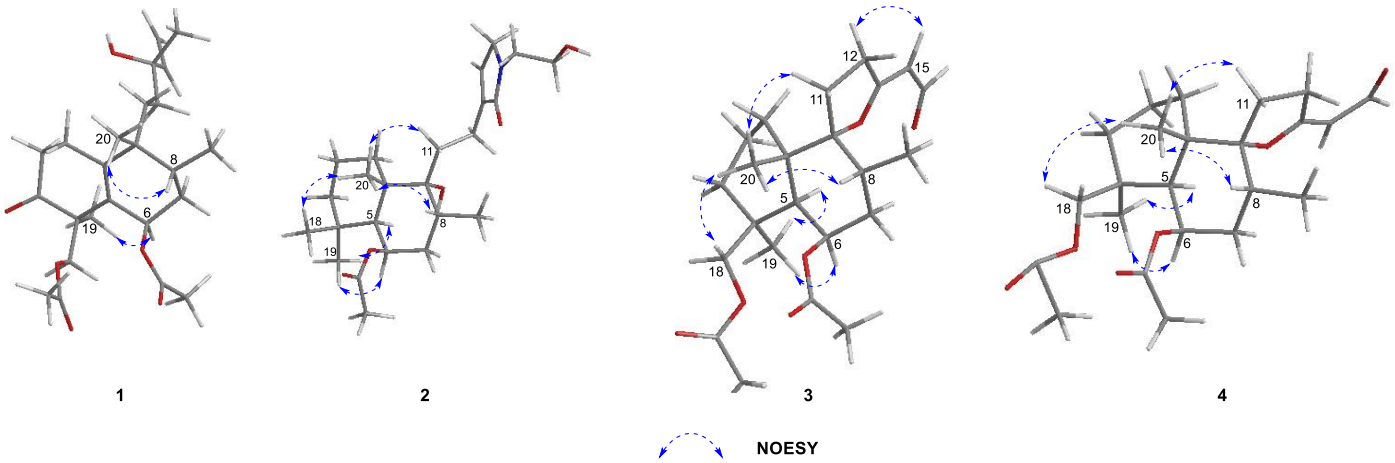

Figure 3 Key NOESY correlations of **1-4**

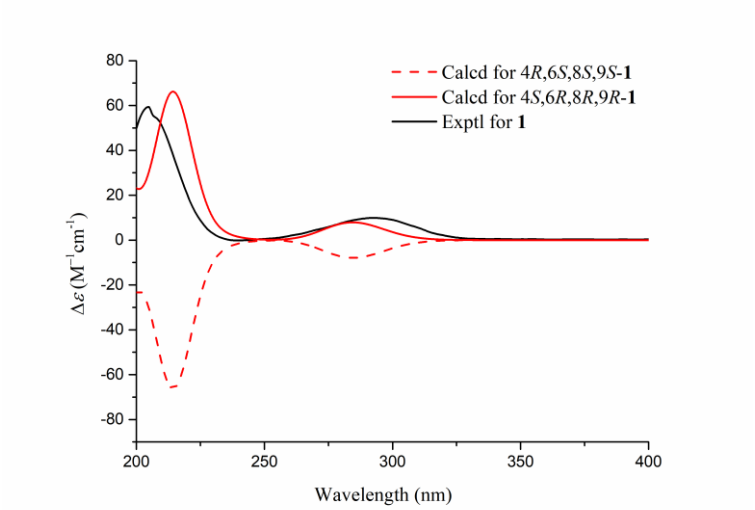

Figure 4 Comparison of the experimental and calculated ECD spectra of **1** (in MeOH).

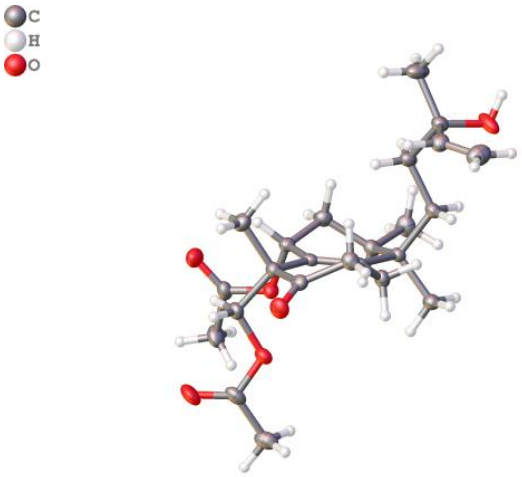

Figure 5 X-ray ORTEP drawing of compound **1** (Cu Kα).

Preprints (www.preprints.org) | NOT PEER-REVIEWED | Posted: 9 May 2023 doi:10.20944/preprints202305.0651.v1

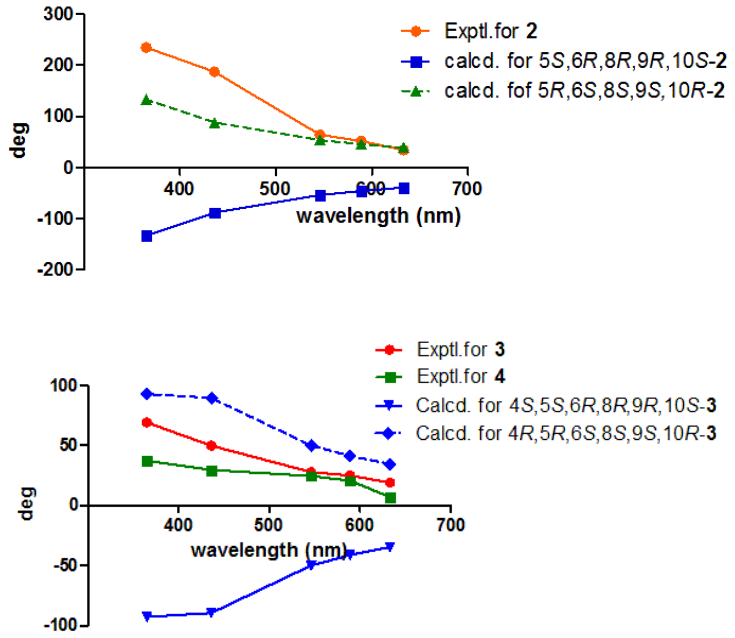

Figure 6 Experimental and calculated ORD spectra of **2-4**

Compound **3** was isolated as a colorless gum. Its molecular formula was determined to be $C_{23}H_{34}O_6$ by HR-ESI-MS data at *m/z* 429.2256 (calcd 429.2253 for $C_{23}H_{34}O_6Na$). The ^1H and ^{13}C NMR data (**Table 2**) of **3** were found to be similar to 6*β*-acetoxy-9*α*,13-epoxy-16-norlabd-13*Z*-en-15-al, previously reported from *L. zeylanica* by our team[11], except for an additional appearance of an acetyl group (δ_H 2.03/δ_C 20.5, δ_C 173.1) and an oxygenated methylene (δ_H 4.48/δ_C 67.6) in **3**, and the absence of a methyl (δ_H 1.05/δ_C 24.0) in 6*β*-acetoxy-9*α*,13-epoxy-16-norlabd-13*Z*-en-15-al. These data indicated that the methyl group in 6*β*-acetoxy-9*α*,13-epoxy-16-norlabd-13*Z*-en-15-al was oxygenated with an acetyl group in **3**. This was supported by the HMBC correlations from H-5 to C-18, H_2-18 to C-3/C-4/C-19 and C-21, Me-19 to C-4/C-5 and C-18, and Me-22 to C-21. The (*Z*)-configuration of the $\Delta^{13(14)}$ double bond was defined by the NOESY correlation of H_2-12/H-14 (**Figure 3**). The relative configuration of **3** was assigned the same as that of 6*β*-acetoxy-9*α*,13-epoxy-16-norlabd-13*Z*-en-15-al, based on the NOESY correlations. The absolute configuration of **3** was established by comparison of their experimental and calculated ORD spectra, which indicated the calculated ORD spectrum (**Figure 6**) of 4*R*,5*R*,6*S*,8*S*,9*S*,10*R*-**3** agreed well with the experimental curve for **3**. Thus, the structure of zeylleucapenoid C (**3**) was established as shown in **Figure 1**.

Compound **4** was isolated as colorless gum. Its molecular formula was determined to be $C_{23}H_{34}O_6$ by HR-ESI-MS data at *m/z* 429.2260 (calcd 429.2253 for $C_{23}H_{34}O_6Na$). The ^{13}C NMR data (**Table 2**) closely resembles that of **3** except for a few deviations of chemical shifts from the signals for C-9 ($\Delta\delta_C$ +1.8), C-11 ($\Delta\delta_C$ −0.9), C-12 ($\Delta\delta_C$ −0.8), C-13 ($\Delta\delta_C$ −3.0), C-14 ($\Delta\delta_C$ −1.0), and C-15 ($\Delta\delta_C$ −2.5) in **4**. Analysis of its 2D NMR spectra showed that **4** is a stereoisomer of **3**. The main differences were the geometrical configuration of the $\Delta^{13(14)}$ double bond. The lack of NOESY correlations observed between H_2-12 and H-14 and the $^3J_{12,14}$ = 2.0 Hz ($^3J_{12,14}$ = 0 Hz in **3**) also verified the $\Delta^{13(14)}$ double bond to be *E*-formed. Because the experimental ORD spectrum (**Figure 6**) of **4** were similar to those of **3**, the absolute configuration of **4** was determined as (4*R*,5*R*,6*S*,8*S*,9*S*,10*R*), and named as zeylleucapenoid D.

Table 2 ^1H and ^{13}C NMR spectral data of compounds **3–4**

Position	3[a]	4[a]

 doi:10.20944/preprints202305.0651.v1

	δ_H, Mult, (*J* in Hz)	δ_C	δ_H, Mult, (*J* in Hz)	δ_C
1	1.25, m; 1.51, m	33.7	1.21, m; 1.48, m	33.7
2	1.55, m; 1.72, m	18.9	1.66, m; 1.53, m	18.9
3	1.89, m; 1.75, m	37.4	1.87, m	37.3
4	-	39.3	-	39.2
5	1.86, d, (2.4)	51.7	1.81, d, (2.4)	51.4
6	5.51, dd, (5.6, 2.8)	70.7	5.48, q, (2.4)	70.7
7	1.75, m; 1.00, m	37.1	1.70, m; 0.97, m	37.0
8	2.24, m	33.2	2.27, m	33.1
9	-	103.3	-	101.5
10	-	44.2	-	43.9
11	2.31, m; 1.98, m	25.8	2.36, m; 2.06, m	26.7
12	2.96, m	30.1	3.20, m	30.9
13	-	183.6	-	186.6
14	5.09, d, (8.8)	100.7	5.55, dt, (8.0, 2.0)	101.7
15	9.86, d, (8.8)	190.7	9.49, d, (8.0)	193.2
17	0.88, d, (6.4)	15.8	0.85, d, (6.4)	15.7
18	4.13, dd, (11.2, 1.6)	67.6	4.41, dd, (11.2, 1.6)	67.6
	4.48, d, (11.2)		4.47, d, (11.2)	
19	1.05, s	27.4	1.03, s	27.4
20	1.33, s	20.7	1.34, s	20.7
21	-	173.1	-	173.1
22	2.03, s	20.5	2.03, s	20.6
23	-	172.0	-	172.0
24	2.10, s	21.8	2.09, s	21.8

[a] measured in CD_3OD at 400 MHz.

2.2. Anti-Inflammatory Activity

Considering the traditional anti-inflammatory efficacy of *L. zeylanica*, compounds **1**-**4** were examined for their ability to inhibit nitric oxide (NO) production [14]. Prior to the bioassay, the *in vitro* cytotoxic effects of against cell viability were detected by the MTT method, and compounds **1**-**4** showed no cytotoxic activity with CC_{50} values of >100 μM. At non-cytotoxic concentrations, compound **4** exhibited significant effects to reduce the LPS-induced NO production with an IC_{50} value of 38.45 μM in RAW264.7 macrophages, while the positive control dexamethasone showed an IC_{50} value of 79.34 μM (**Figure 7**). Meanwhile, the zebrafish embryo toxicity test was thought to be suitable for evaluation of the toxic property of drug candidates. Herein, the active compound **4** was evaluated toxicity effects with zebrafish embryo model, which indicated that **4** showed nontoxic activity at the concentrations of 12.5, 50 and 100 μM, respectively (**Figure 8**). Subsequent ELISA assay uncoverred **4** could strongly suppress the secretion of LPS-induced TNF-α and IL-6 cytokines in a dose-dependent manner for RAW264.7 macrophages (**Figure 9**). In order to understand the possible anti-inflammatory mechanism, the effects of **4** on iNOS and COX-2 protein expression levels were examined by Western blotting, which indicated compound **4** was shown to dose-dependently attenuate the inflammatory mediator iNOS and COX-2 levels (**Figure 10**). On the base above, these data disclosed compound **4** played an important role through the down regulating of pro-inflammatory enzyme expression, leading to an anti-inflammatory effect.

Preprints (www.preprints.org) | NOT PEER-REVIEWED | Posted: 9 May 2023 doi:10.20944/preprints202305.0651.v1

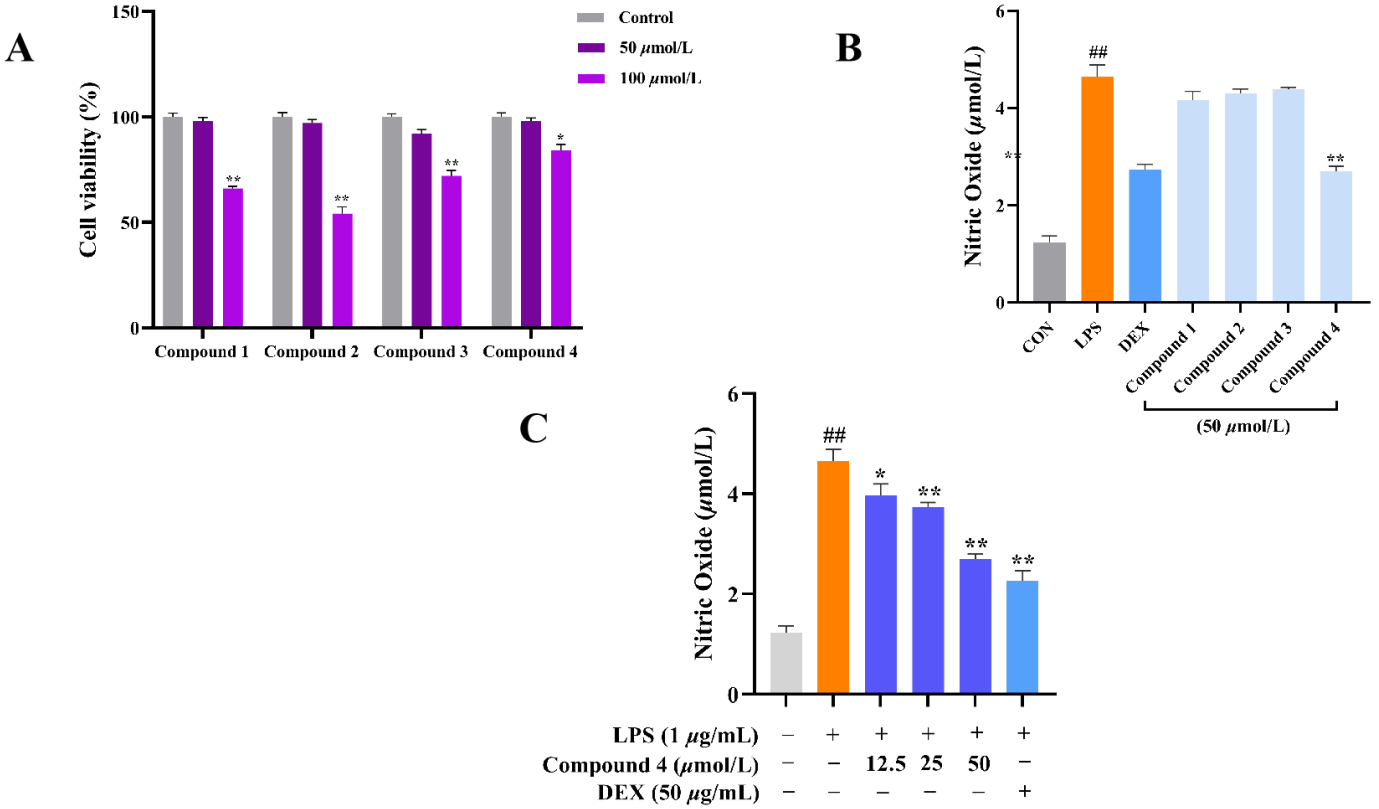

Figure 7 The effects of the administered dose of the compounds **1-4** on cell viability and NO levels were determined. (A) Cell viability of compounds **1-4** at the dose of 50, 100 μM. *$p < 0.05$, **$p < 0.01$ vs. Con. n ≥ 3. (B) The levels of NO in LPS induced RAW264.7 macrophages at a concentration of 50 μM for samples. (C) Compound **4** reduce LPS induced RAW264.7 macrophages NO levels. ##$p < 0.01$ vs. Con, *$p < 0.05$, **$p < 0.01$ vs. LPS. n ≥ 3.

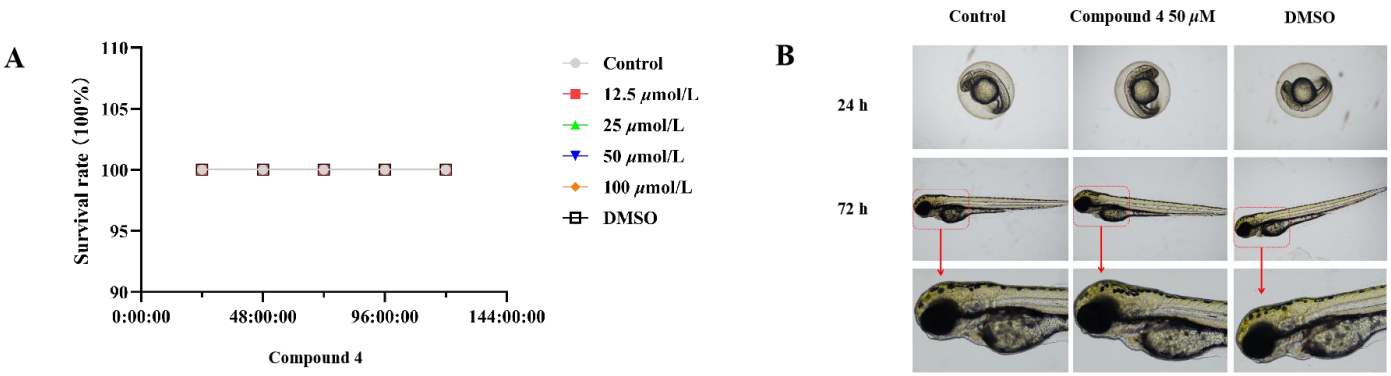

Figure 8 The toxicity effect of compound **4** in zebrafish. (A) The toxicity of compound **4** were used to test with zebrafish model. At 1-5 dpf, zebrafish embryos were subjected to different compound concentrations (12.5, 25, 50, 100 μM). The number of dead embryos were recorded every day. (B) Effect of compound **4** on the development and morphology of zebrafish embryos.

Preprints (www.preprints.org) | NOT PEER-REVIEWED | Posted: 9 May 2023 doi:10.20944/preprints202305.0651.v1

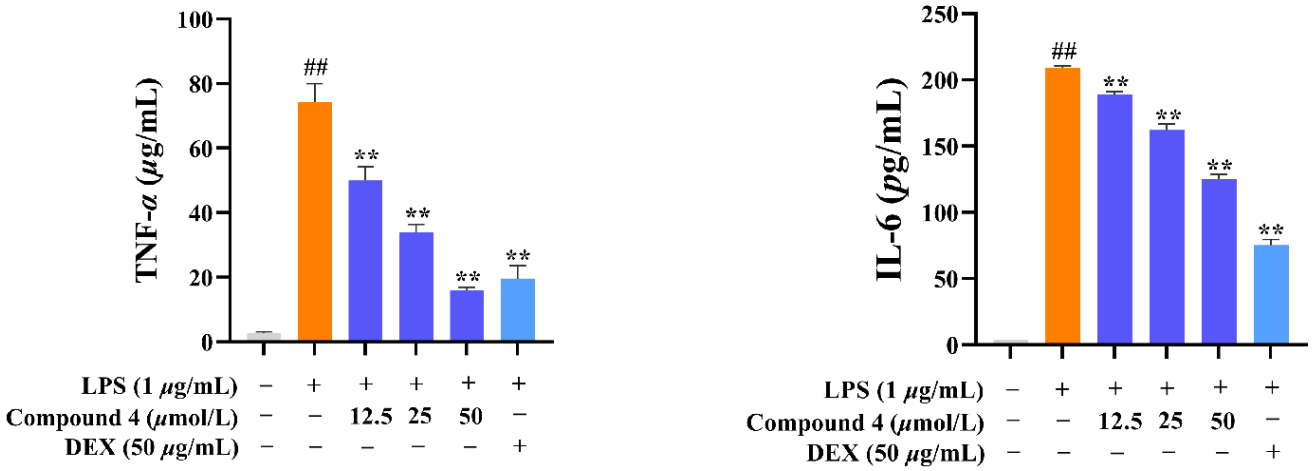

Figure 9 Impact of compound **4** on cytokine secretion in LPS-treated RAW264.7 cells. Cell pre-treatment was done for 1 h using different concentrations for compound **4** concentrations (12.5, 25, and 50 μM) followed by LPS (1 μg/mL) treatment for 24 h. Supernatants of the cell cultures were obtained and used to determine IL-6 and TNF-α levels by ELISA. $^{\#\#}p < 0.01$ vs. Con, $^{**}p < 0.01$ vs. LPS. n ≥ 3.

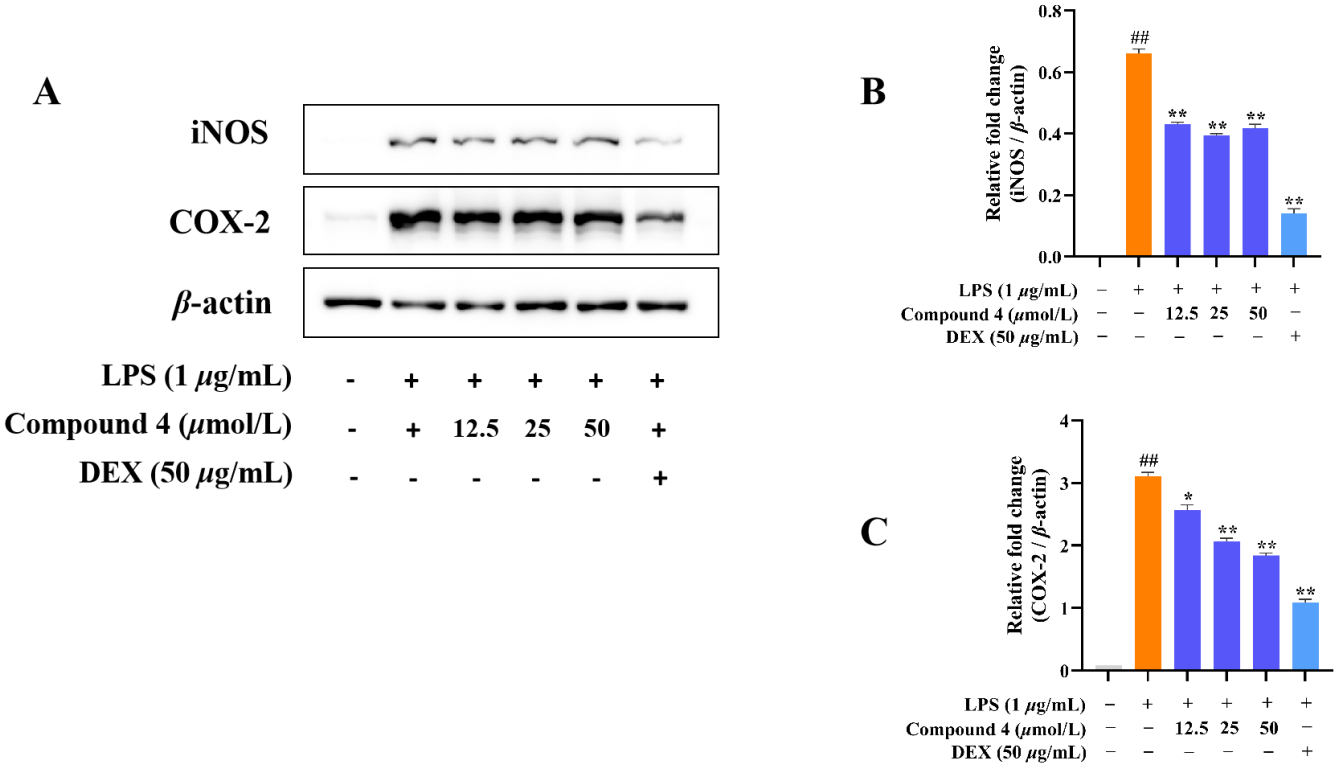

Figure 10 Inhibition of LPS-induced iNOS and COX-2 gene expression in RAW264.7 cells for compound **4**. RAW264.7 cells were preincubated using compound **4** for 1 h, followed co-treated with LPS for 24 h, and analysed by western blotting. (A) Western blotting; (B) iNOS expression; (C) COX-2 expression. Data were expressed as mean ± SD (n ≥ 3). $^{\#\#}p < 0.01$ vs. Con, $^{*}p < 0.05$, $^{**}p < 0.01$ vs. LPS. n ≥ 3.

*2.3. Predicted Binding Modes of Compound **4** and both iNOS and COX-2 Using Molecular Docking Analysis*

Preprints (www.preprints.org) | NOT PEER-REVIEWED | Posted: 9 May 2023 doi:10.20944/preprints202305.0651.v1

To further recognize the possible binding modes of anti-inflammatory activity for **4**, a molecular docking study was performed between **4** and both iNOS and COX-2 proteins. The result showed that **4** was well accommodated in the binding pocket of iNOS, and primarily interacted with Tyr341 and Arg375 residues through stable hydrogen bonds, and interacted with residues Trp84 and Val346 through hydrophobic bonds, respectively (**Figure 11**). Meanwhile, in the binding pocket of COX-2, compound **4** mainly formed stable hydrogen bonds with Tyr348, Val523 and Arg120 residues, and formed hydrophobic bonds with residues Val523 and Tyr355, respectively (**Figure 11**). The lower binding energies with -5.862 and -6.722 kcal/mol, respectively, also provided reliable evidence to confirm their strong affinity (**Table 4**). Therefore, the molecular docking analysis provided a perspective about the potential targets for **4**, which will be helpful to discover the specific binding site by follow-up experiment.

Table 4 Logarithms of free binding energies (FBE, kcal/mol) between compound **4** and the active cavities of both iNOS (PDB code, 3E6T) and COX-2 (PDB code, 1PXX) via targeting residues.

Compounds	Protein	-Log(FBE)	Targeting Residues			
4	iNOS	-5.862	Tyr341	Arg375	Trp84	Val346
	COX-2	-6.722	Tyr348	Val523	Arg120	Tyr355

3. Materials and Methods

3.1 General experimental procedures

The optical rotation value was tested through a JASCO P-1020 digital polari meter, while the acquisition of ECD spectra were through a Jasco J-815 circular dichroism spectrometer at room temperature. 1D, 2D-NMR data were recorded on a Bruker AV spectrometer (400 MHz for ^{1}H and 100 MHz for ^{13}C), while TMS was used as an internal reference. The acquisition of HRESIMS data was via a Q-TOF Ultima Global GAA076 LC mass spectrometer. Semi-preparative HPLC was carried out on an Agilent 1260 LC infinity series, by loading an Agilent Eclipse XDB-C_{18} column (9.4 × 250 mm, 5 μm), using a DAD-UV detector. Silica gel (Qing Dao Hai Yang Chemical Group Co.; 100-200, 200-300 mesh) were employed in column chromatography (CC). Thin-layer chromatography (TLC) (Yan Tai Zi Fu Chemical Group Co.; G60, F-254) were used for monitor the separation of samples. Anti-inflammatory activity was evaluated by using Microplate spectrophotometer (BD, Bioscience USA) as a template reader.

3.2. Plant material

The aerial parts of *Leucas zeylanica* (Lamiaceae) was collected from Changjiang city, Hainan province of China in July 2020, and were authenticated by Professor Yu-Kai Chen (School of Hainan Normal University, Hainan, China). The specimens (No C20-L02) were deposited at the Key Laboratory of Tropical Medicinal Resource Chemistry of Ministry of Education, Hainan Normal University (Hainan, China).

3.3. Extraction and Isolation:

The aerial parts of *L. zeylanica* (10.0 kg) was extracted with 95% EtOH (3 × 25 L). A dark brown crude extract (1.1 kg) was obtained after concentration in vacuo to remove most of the EtOH. The crude extract was suspended in distilled water and partitioned with PE (60-90) (3.0 × 1.0 L), EtOAc (3.0 × 1.0 L) and *n*-BuOH (3.0 × 1.0 L), yielding 90, 295 and 354 g of residues, respectively.

The PE-soluble fraction (87 g) was subjected to silica gel column chromatography (CC) (100-200 mesh) with gradient elution (petroleum ether/ethyl acetate, 100:0, 90:10, 80:20, 70:30, 60:40, 0:100; *v/v*, each 6 L) to afford four major fractions (Fr. P1-P4).

The Fr. P-3 (15 g) part was separated by a silica gel column and eluted with gradient mixtures of petroleum ether-acetone (from 5:1 to 1:1) to obtain fractions (Fr. P3-1-P3-5). Fraction Fr. P3-3 (6 g) was separated on Sephadex LH-20 ($CHCl_3$: MeOH, 1:1) and a RP-C_{18} silica gel column (MeOH/H_2O, from 70% to 100%) to obtain fractions Fr. P33-1-P33-6

Preprints (www.preprints.org) | NOT PEER-REVIEWED | Posted: 9 May 2023 doi:10.20944/preprints202305.0651.v1

on the basis of TLC analysis. Fraction Fr. P3.3-3 (160 mg) was purified by semi-preparative HPLC with (MeOH/H_2O, 60:40 *v*/*v*) as eluent to afford compound **1** (12 mg).

The EtOAc-soluble fraction (290 g) was subjected to silica gel column chromatography (CC) (100-200 mesh) with gradient elution (petroleum ether/ethyl acetate and chloroform/methanol, 100:0, 90:10, 80:20, 70:30, 60:40, 0:100; *v*/*v*, each 8 L) to afford six major fractions (Fr. E1-E2).

Fr. E-3 (24.2 g) was subjected to an ODS column and eluted with MeOH/H_2O (from 10:90 to 100:0 *v*/*v*), attaining seven sub-fractions (Fr. E3-1-Fr. E3-7). Fr. E3-3 (1.7 g) was purified on a silica gel column (200-300 mesh, petroleum ether-EtOAc, 100:0, 90:10, 80:20, 70:30, 60:40, 0:100 *v*/*v*) to yield five additional fractions (Fr. E33-1-Fr. E33-5). Fr. E33-3 (336 mg) was decolorized by a silicone column and eluted by gradient elution (MeOH-H_2O, from 80:20 to 100:0 *v*/*v*), to yield three subfractions (Fr. E333-1-Fr. E333-3). Compounds **3** (2.1 mg) and **4** (5.6 mg) were obtained from Fr. E333-2 (87 mg) by HPLC (MeOH-H_2O, 61:39 *v*/*v*).

Fr. E-5 (1.2 g) was subjected to silica gel column chromatography (CC) (200-300 mesh) using $CHCl_3$-MeOH (100:0, 90:10, 80:20, 70:30, 60:40, 0:100; *v*/*v*) with gradient elution to afford five fractions (Fr. E5-1-Fr. E5-5). Fr. E5-3 (540 mg) was subjected to an ODS column eluting with MeOH/H_2O (from 20:80 to 100:0 *v*/*v*,) to obtain four subfractions (Fr. E53-1-Fr. E53-4). Fr. E53-3 (118 mg) further purified by HPLC (MeOH-H_2O, 68:32) to obtain compound **2** (7.8 mg).

*3.3.1. Zeylleucapenoid A (**1**):*

colorless block crystals; $[\alpha]^{25}_D$ +11.43 (*c* 0.14, MeOH); mp 156.6-157.9 °C; UV (MeOH) λ_{max} (log ε) 220 (3.91), 266 (3.02), 275 (2.95) nm; CD (*c* 0.0005, MeOH) λ_{max} ($\Delta\varepsilon$) 205 (+59.40), 293 (+9.90) nm; ^{1}H NMR (400 MHz, CD_3OD) and ^{13}C NMR (100 MHz, CD_3OD), see **Table 1**; HR-ESI-MS *m*/*z* 443.2415 (calcd 444.2410 for $C_{24}H_{36}O_6Na$).

3.3.2. Zeylleucapenoid B (**2**):

white powder; $[\alpha]^{25}_D$ +51.7 (*c* 2.1, MeOH); UV (MeOH) λ_{max} (log ε) 222 (3.99), 306 (3.02), 318 (2.93) nm; ^{1}H NMR (400 MHz, CD_3OD) and ^{13}C NMR (100 MHz, CD_3OD), see **Table 1**; HR-ESI-MS *m*/*z* 444.2725 (calcd 444.2726 for $C_{24}H_{39}NO_5Na$).

*3.3.3. Zeylleucapenoid C (**3**):*

colorless gum; $[\alpha]^{25}_D$ +24.84 (*c* 1.0, MeOH); UV (MeOH) λ_{max} (log ε) 220 (3.90), 266 (3.25) nm; ^{1}H NMR (400 MHz, CD_3OD) and ^{13}C NMR (100 MHz, CD_3OD), see **Table 2**; HR-ESI-MS *m*/*z* 429.2256 (calcd 429.2253 for $C_{23}H_{34}O_6Na$).

*3.3.4. Zeylleucapenoid D (**4**):*

colorless gum; $[\alpha]^{25}_D$ +20.53 (*c* 1.5, MeOH); UV (MeOH) λ_{max} (log ε) 219 (3.95), 267 (3.69) nm; ^{1}H NMR (400 MHz, CD_3OD) and ^{13}C NMR (100 MHz, CD_3OD), see **Table 2**; HR-ESI-MS *m*/*z* 429.2260 (calcd 429.2253 for $C_{23}H_{34}O_6Na$).

3.4. X-ray crystallographic analysis

Crystals of compound **1** was obtained from MeOH at room temperature. Single-crystal X-ray diffraction data were collected on a Rigaku, Oxford diffractometer with Cu Kα radiation (λ = 1.54184 Å) at 100.00(10) K, respectively. Using the direct methods (ShelXS) and refined with the ShelXL program, structure determination and refinement were performed. Crystallographic data of compound **1** has been deposited with the Cambridge Crystallographic Data Centre (CCDC numbers: 2225700 for **1**). The data can be obtained free of charge from the Cambridge Crystallographic Data Centre (https://www.ccdc.cam.ac.uk/).

Crystal data of compound **1**: $C_{24}H_{36}O_6$, M_r = 420.53; colorless block crystals from CH_3OH; crystal size = 0.25 × 0.16 × 0.14 mm^3; T = 100.00(10) K; space group $P2_1$; monoclinic, *a* = 9.33510 (10) Å, *b* = 9.69210 (10) Å, *c* = 13.5574 (2) Å, α = 90°, β = 107.5540(10), γ = 90°, *V* = 1169.51(3) Å^3, *Z* = 2, D_{calc} = 1.194 g/cm^3, *F* (000) = 456.0, μ (Cu Kα) = 0.685 mm^{-1}. Independent reflections: 4731 unique (R_{int} = 0.0227, R_{sigma} = 0.0194). The final R_1 was 0.0288 and wR_2

Preprints (www.preprints.org) | NOT PEER-REVIEWED | Posted: 9 May 2023 doi:10.20944/preprints202305.0651.v1

was 0.0751 [I >= 2σ (I)] (all data). Flack parameter = 0.00(5). CCDC no. 2225700 (**Table S1** in the Supporting Information).

3.5. Anti-Inflammatory Activity:

3.5.1 NO measurement

All isolated compounds were evaluated for their inhibition of nitric oxide (NO) production in RAW264.7 cells activated by lipopoly saccharide (LPS) using the Griess assay with dexamethasone (DEX) as a positive control[15-16]. RAW 264.7 cells were seeded in 96-well plates at a density of 2 × 10^5 cells/mL. After 12 h of incubation, the cells were pretreated with compounds (50 μM) and DEX (50 μg/mL) for 1 h and following LPS (1 μg/mL) additional treatment for 24 h at 37°C. After 24 h, the quantity of NO accumulated in the culture medium was measured. Briefly, cell culture medium (50 μL) was added with equivalent volume of the Griess reagent. The absorbance was measured by a microplate reader at 540 nm wavelength.

3.5.2 The MTT assay

Briefly, RAW264.7 cells were seeded in 96-well plates at a density of 1 × 10^5 cells/mL. Incubation was performed for 12 h after which compounds (50 μM) was used to treat the cells for 24 h. Subsequently, 20 μL of the MTT stock solution (5 mg/mL) was added to wells. After 4 h incubation, the supernatants were aspirated. The formazan crystals in each well were dissolved in DMSO (150 μL), and the absorbance was measured with the wavelength of 570 nm by a microplate reader. The data were expressed as mean percentages of the viable cells compared to the respective control.

3.5.3 Zebrafish maintenance

Adult wild-type zebrafish (Danio rerio) were raised at a standard facility, which may control stationary light and temperature. The zebrafish were treated with light/dark photoperiod at 14:10 h cycles, and fed by live brine shrimp for 2 times a day. Further the embryos were produced from the spawning of adult fish using a hatch box, and the incubation process from embryo to larvae was maintained at 28°C. The larvae were collected and used for the toxic experiments. All the zebrafish procedures were approved by the Institutional Animal Care and Committee of Hainan Normal University.

3.5.4 Toxic effects in zebrafish

Although the anti-inflammatory activity of diterpenoids in zebrafish models has been reported previously[17-19], it is still not very common. Compound **4** was evaluated for zebrafish larval toxicity studies. Four h post-fertilization (hpf) larvae were placed in 6 well plates at a count of 10 fish/well and compounds was added in the fish water at 4 different concentrations (12.5, 25, 50, 100 μM). The EVOS digital microscope (4x) was used to detect toxicities activity for the larval zebrafish up to 120 hpe (hour post exposure). Prior to the test, larval zebrafish were checked their viability, where the death was often considered to lack of a heartbeat (acute toxic dose). Other indications of toxicity involved in swim position, and morphological deficits such as malformations, larval length, tail curvature, and swim bladder inflation level.

3.5.5 ELISA assay

Cytokine levels were quantified using ELISA kits according to the manufacturer's protocol[20-21]. After pretreatment with compound **4** (12.5, 25 and 50 μM, respectively) and DEX (50 μg/mL) for 1 h, cells were incubated with compound **4** and LPS for an additional 24 h, and cell culture supernatants were collected. The expression levels of IL-6 and TNF-α in the culture medium were assessed by measuring the absorbance at 450 nm using a microplate reader.

3.5.6 Western Blot Analysis

RAW264.7 cells were seeded at a density of 1 x 10^6 cells/well in 6-well plates for 24 hours[22-23]. Cells were then pretreated with compound **4** for 1 h and stimulated with LPS (1 μg/mL). After 24 hours of continuous incubation, cells were washed twice with cold

 doi:10.20944/preprints202305.0651.v1

PBS and collected. Cells were lysed with lysis buffer containing freshly added protease inhibitor cocktail and phenylmethyl sulfonylfluoride. The lysate was then centrifuged at 12,000 rpm for 10 minutes and the supernatant was collected to obtain total protein. Protein concentrations were determined using the BCA Protein Assay Kit (Beyotime Biotechnology). Equal amounts of protein were separated by SDS-PAGE gel electrophoresis and transferred to polyvinylidene difluoride membranes. Membranes were blocked with 5% skimmed milk for 2 h at room temperature and then membranes were further incubated with primary antibody (iNOS and COX-2) at 4℃ overnight followed by incubation with horseradish peroxidase conjugated secondary antibody. Finally, protein blots were visualised using an ECL detection kit (Beyotime Biotechnology). β-actin was used as an internal reference. Each band was quantified using Image J software.

3.5.7 Molecular docking studies

Molecular docking was conducted in AutoDock using the hybrid Lamarckian Genetic Algorithm (LGA)[24-25]. The 3D structure of iNOS (PDB:3E6T) and COX-2 (PDB:1PXX) was download from RCSB PDB (https://www.rcsb.org/). The 3D structure of **4** was drawed by ChemDraw (https://www.chemdraw.com.cn/) as ligands. The protein and ligand were converted to PDBQT format using AutoDock Tools. The ligands was set to flexible; the receptor was set to rigid. The conformation with the lowest binding free energy was finally identified as the best probable binding mode. Water molecules and original ligand of the receptor was manually removed by using PyMol software. Prepare_ligand4.py and prepare_recptor4.py scripts from AutoDockTools 1.5.6 were used to prepare the initial files of ligands including adding charges and hydrogen atoms.

4. Conclusions

Chemical investigations of the 95% EtOH extract of *L. zeylanica* afforded four undescribed highly oxygenated halimane-type and labdane-type diterpenoids (**1–4)**. The absolute configuration of the new compound **1** is determined by theoretical ECD calculations and single crystal diffraction. The absolute configuration of the new compounds **2**-**4** is determined by theoretical ORD calculations. Among them, compound **4** showed significant anti-inflammatory activity against LPS-induced NO, TNF-α and IL-6 production, and inhibition of iNOS and COX-2 protein expression levels. The molecular docking analysis indicated that **4** had strong affinity with both iNOS and COX-2 through hydrogen- and hydrophobic- bond interaction with a few amino acid residues. These results were significative for the discovery of anti-inflammatory target and lead compounds for treatment of inflammation-linked diseases.

Supplementary The following supporting information can be downloaded at the website of this paper posted on Preprints.org. Table S1 Crystal data and structure refinement for compound **1** autored. Table S2 Fractional Atomic Coordinates (×10^4) and Equivalent Isotropic Displacement Parameters (Å2×10^3) for compound **1** autored. Ueq is defined as 1/3 of of the trace of the orthogonalised UIJ tensor. Table S3 Anisotropic Displacement Parameters (Å2×103) for LE35113_A_autored. The Anisotropic displacement factor exponent takes the form: -2π2[h2a*2U11+2hka*b*U12+…]. Table S4 Bond Lengths for compound **1** autored. Table S5 Bond Angles for compound **1** autored. Table S6 Hydrogen Bonds for compound **1** autored. Table S7 Torsion Angles for compound **1** autored. Table S8 Hydrogen Atom Coordinates (Å×10^4) and Isotropic Displacement Parameters (Å2×10^3) for compound **1** autored. Computational Section. Table S9 Energies of the dominative conformers of compound **1**. Table S10 Energies of the dominative conformers of compounds **2** and **3**. Table S11 Calculated and measured OR values of compounds **2** and **3** at different wavelengths. Table S12 The docking pockets. Figure S1 The UV Spectrum of Compound **1**. Figure S2 The (+)-HRMS(ESI) Spectroscopic Data of Compound **1**. Figure S3 The ^{1}H NMR Spectrum of Compound **1** in CD_3OD. Figure S4 The ^{13}C NMR Spectrum of Compound **1** in CD_3OD. Figure S5 The DEPT Spectrum of Compound **1** in CD_3OD. Figure S6 The HSQC Spectrum of Compound **1** in CD_3OD. Figure S7 The ^{1}H-^{1}H COSY Spectrum of Compound **1** in CD_3OD. Figure S8 The HMBC Spectrum of Compound **1** in CD_3OD. Figure S9 The NOESY Spectrum of Compound **1** in CD_3OD. Figure S10 The UV Spectrum of Compound **2**. Figure S11 The (+)-HRMS(ESI) Spectroscopic Data of Compound **2**. Figure S12 The ^{1}H NMR Spectrum of Compound **2** in DMSO-d_6. Figure S13 The ^{13}C

 doi:10.20944/preprints202305.0651.v1

NMR Spectrum of Compound **2** in DMSO-d_6. Figure S14 The DEPT Spectrum of Compound **2** in DMSO-d_6. Figure S15 The HSQC Spectrum of Compound **2** in DMSO-d_6. Figure S16 The ^{1}H-^{1}H COSY Spectrum of Compound **2** in DMSO-d_6. Figure S17 The HMBC Spectrum of Compound **2** in DMSO-d_6. Figure S18 The NOESY Spectrum of Compound **2** in DMSO-d_6. Figure S19 The UV Spectrum of Compound **3**. Figure S20 The (+)-HRMS(ESI) Spectroscopic Data of Compound **3**. Figure S21 The ^{1}H NMR Spectrum of Compound **3** in CD_3OD. Figure S22 The ^{13}C NMR Spectrum of Compound **3** in CD_3OD. Figure S23 The DEPT Spectrum of Compound **3** in CD_3OD. Figure S24 The HSQC Spectrum of Compound **3** in CD_3OD. Figure S25 The ^{1}H-^{1}H COSY Spectrum of Compound **3** in CD_3OD. Figure S26 The HMBC Spectrum of Compound **3** in CD_3OD. Figure S27 The NOESY Spectrum of Compound **3** in CD_3OD. Figure S28 The UV Spectrum of Compound **4**. Figure S29 The (+)-HRMS(ESI) Spectroscopic Data of Compound **4**. Figure S30 The ^{1}H NMR Spectrum of Compound **4** in CD_3OD. Figure S31 The ^{13}C NMR Spectrum of Compound **4** in CD_3OD. Figure S32 The DEPT Spectrum of Compound **4** in CD_3OD. Figure S33 The HSQC Spectrum of Compound **4** in CD_3OD. Figure S34 The ^{1}H-^{1}H COSY Spectrum of Compound **4** in CD_3OD. Figure S35 The HMBC Spectrum of Compound **4** in CD_3OD. Figure S36 The NOESY Spectrum of Compound **4** in CD_3OD.

Author Contributions: T.Z. and X.Z. performed the bioassay, analyzed the data, and wrote the manuscript. G.-Y.C., X.-B.L. T.Z. X-.H.N. X.-M.Z. and R.-R.C. conducted the isolation and structure elucidation of the constituents. T.Z. X.-B.L. and G.-Y.C. planned, designed, and organized all of the research for this study and prepared the manuscript. All authors have read and agreed to the published version of the manuscript.

Funding: Supported by the specific research fund of the Key R&D Projects in Hainan Province-Social Development (ZDYF2021SHFZ072), the National Natural Science Foundation of China (No. 21662012), the Innovation Platform for Academicians of Hainan Province (YSPTZX202030), and the Central Government Guides Local Science and Technology Development (No. ZY2022HN08) and and the Innovative research project of Hainan Graduate students (Qhyb2022-105, RC2100006644).

Institutional Review Board Statement: Not applicable.

Informed Consent Statement: Not applicable.

Data Availability Statement: The data of the article can be obtained from the authors.

Conflflicts of Interest: The authors declare no conflflict of interest.

Sample Availability: Not available.

References

1. Hunter, P. The inflammation theory of disease. *Science & Society*. **2012**, *11, 968-970.*
2. Zeinali, M., Rezaee, S.A., Hosseinzadeh, H. An overview on immunoregulatory and anti-inflammatory properties of chrysin and flavonoids substances. *Biomed. Pharmacother*. **2017**, *92, 998-1009*.
3. Hanson, J.R., Nichols, T., Mukhrish, Y., Bagley, M.C. Diterpenoids of terrestrial origin. *Nat. Prod. Rep*. **2019**, *36, 1499-1512.*
4. Wang, X.L., Yu, H.B., Zhang, Y.X., Lu, X.L., Wang, B., Liu, X.Y. Bioactive pimarane-type diterpenes from *Marine organisms*. *Chem. Biodivers*. **2017**, *15, 1-12.*
5. Xu, Y., Tang, P.Y., Zhu, M., Wang, Y.L., Sun, D.J., Li, H., Chen, L.X. Diterpenoids from the genus Euphorbia: structure and biological activity (2013-2019). *Phytochemistry*. **2021**, *190, 112846.*
6. Zhan, Z.J., Li, S., Chu, W., Yin, S. Euphorbia diterpenoids: isolation, structure, bioactivity, biosynthesis, and synthesis (2013-2021). *Nat. Prod. Rep.* **2022**, *39, 2132-2174.*
7. Naidoo, Y., Dladla, T., Dewir, Y.H., Gangaram, S., Naidoo, C.M., Rihan, H.Z. The micromorphology and histochemistry of foliar mixed indumentum of *Leucas lavandulaefolia* (Lamiaceae). *Plants*. **2021**, *10, 1767-1778.*
8. Shurpali, R.R.K.K., Sarkar, V.G.P.D., Joshi, S.P. Antimycobacterial labdane diterpenes from *Leucas stelligera*. *J. Nat. Prod.* **2013**, *76, 1836-1841.*
9. Zhang, X.P., Zhang, C.Y., Chen, C.Y., Yu, L., Liu, J. Leucasinoside: A new abietane diterpenoid glycoside from *Leucas zeylanica*. *Rec. Nat. Prod.* **2016**, *10, 645-648.*
10. Shahdat, H., Mijanur, R., Nusrat, F., Mozammel, H., Jahirul, I. *Leucas zeylanica* (L.) R. Br. protects ethanol and hydrogen peroxide-induced oxidative stress on hepatic tissue of rats. *International Current Pharmaceutical Journal*, **2013**, *2, 148-151.*
11. Nidhal, N., Zhou, X.M., Chen, G.Y., Zhang, B., Han, C.R., Song, X.P. Chemical constituents of *Leucas zeylanica* and their chemotaxonomic significance. *Biochem. Syst. Ecol.* **2020**, *89, 10400.*
12. Sadhu, S.K., Okuyama, E., Fujimoto, H., Ishibashi, M. Diterpenes from *Leucas aspera* inhibiting prostaglandin-induced contractions. *J. Nat. Prod*. **2006**, *69, 988-994.*

13. Li, S.H., Zhang, H.J., Qiu, S.X., Niu, X.M., Santarsierod, B.D., Mesecard, A.D., Fong, H.H.S., Farnsworth, N.R., Sun, H.D. Vitexlactam A, a novel labdane diterpene lactam from the fruits of *Vitex agnus-castus*. *Tetrahedron Lett*. **2002**, *43, 5131-5134*.
14. Tilg, H., Moschen, A.R. Adipocytokines: mediators linking adipose tissue, inflammation and immunity. *Nat. Rev. Immunol*. **2006**, *6, 772-783*.
15. Wang, S.K., Chen, T.X., Wang, W., Xu, L.L., Zhang, Y.Q., Jin, Z., Liu, Y.B., Tang, Y.Z. Aesculetin exhibited anti-inflammatory activities through inhibiting NF-κB and MAPKs pathway *in vitro* and *in vivo*. *J Ethnopharmacol*. **2022**, *296, 115489.*
16. Guo, H., Wu, Q.L., Chen, D.N., Jiang, M.H., Chen, B., Lu, Y.J., Li, J., Liu, L., Chen, S.H. Absolute configuration of polypropionate derivatives: Decempyrones A-J and their MptpA inhibition and anti-inflammatory activities. *Bioorg. Chem.* **2021**, *115, 105156*.
17. Zhou, X., Cao, C.Y., Wan, A.T.Y., Yue, G.G.L., Kwok, F.H.F., Funget, K.P., Sun, H., Lau, C.B.S., Puno, P.T., Tsuial, S.K.W. Functional roles of eriocalyxin B in zebrafish revealed by transcriptome analysis. *Molecular Omics*. **2018**, *14, 156-169.*
18. Haneen, A., Noor, A.H., Chandrabose, K., Elangovan, M., Alexander, W., Frederick, E.W., Temesgen, S., Piyush, T., Charies, R.A., Amit. K.T. HM015k, a novel silybin derivative, multi-targets metastatic ovarian cancer cells and is safe in zebrafish toxicity studies. *Front. Pharmacol.* **2017**, *8, 498-515.*
19. Liu, Y., Zhang, X., Zhang, J.P., Zhang, J.P., Hu, C.Q. Construction of a quantitative structure activity relationship (QSAR) model to predict the absorption of cephalosporins in zebrafifish for toxicity study. *Front. Pharmacol.* **2019**, *10, 1-10.*
20. Chen, J., Li, D.L., Xie, L.N., Ma, Y.R., Wu, P.P., Li, C., Liu, W.F., Zhang, K., Zhou, R.P., Xu, X.T., Zheng, X., Liu, X. Synergistic anti-inflammatory effects of silibinin and thymol combination on LPS-induced RAW264.7 cells by inhibition of NF-κB and MAPK activation. *Phytomedicine*. **2020**, *78, 153309.*
21. Zhen, D., Xuan, T.Q., Hu, B.Q., Bai, X., Fu, D.N., Wang, Y., Wu, Y., Yang, J.F., Ma, Q.Q. Pteryxin attenuates LPS-induced inflammatory responses and inhibits NLRP3 inflammasome activation in RAW264.7 cells. *J Ethnopharmacol.* **2022**, *284, 114753.*
22. Huang, X.C., Wang, M., Wang, C.G., Hu, W.W., You, Q.H., Yang, Y., Yu, C.H., Liao, Z.X., Gou, S.H., Wang, H.S., Dual-targeting antitumor conjugates derived from platinum (IV) prodrugs and microtubule inhibitor CA-4 significantly exhibited potent ability to overcome cisplatin resistance. *Bioorg. Chem*. **2019**, *92, 103236-103236.*
23. Yang, Y.L., Yang, X.Y., Zhang, X.K., Song, Z.T., Liu, F., Liang, Y., Zhang, J., Jin, D.Q., Xu, J., Lee, D., Tuerhong, M., Ohizumi, Y., Guo, Y.Q. Bioactive terpenoids from *Euonymus verrucosus var. pauciflorus* showing NO inhibitory activities. *Bioorg. Chem*. **2019**, *87, 447-456.*
24. Xi, Y., An, L.J., Yang, X.Y., Song, Z.T., Zhang, J., Tuerhong, M., Jin, D.Q., Ohizumi, Y., Lee, D., Xu, J., Guo, Y.Q. NO inhibitory phytochemicals as potential anti-inflammatory agents from the twigs of *Trigonostemon heterophyllus*. *Bioorg. Chem*. **2019**, *87, 417-424.*
25. Trott, O., Olson, A.J. AutoDock Vina: improving the speed and accuracy of docking with a new scoring function, efficient optimization, and multithreading. *J Comput Chem.* **2010**, *31, 455-461.*